HHS Public Access

Author manuscript

Nat Commun. Author manuscript; available in PMC 2015 January 31.

Published in final edited form as:

Nat Commun. ; 5: 4511. doi:10.1038/ncomms5511.

SOX2 is a cancer-specific regulator of tumor initiating potential in cutaneous squamous cell carcinoma

Jasmin M. Siegle[1], **Alice Basin**[1], **Ana Sastre-Perona**[1], **Yoshiya Yonekubo**[1], **Jessie Brown**[1], **Rachel Sennett**[3], **Michael Rendl**[3], **Aristotelis Tsirigos**[2], **John A. Carucci**[1], and **Markus Schober**[1,*]

[1]Ronald O. Perelman Department of Dermatology, Department of Cell Biology, Martin and Helen Kimmel Center for Stem Cell Biology, Perlmutter Cancer Center, New York University Langone Medical Center, New York, NY

[2]Department of Pathology, Center for Health Informatics and Bioinformatics, New York University Langone Medical Center, New York, NY

[3]Black Family Stem Cell Institute, Department of Developmental and Regenerative Biology, Department of Dermatology, Icahn School of Medicine at Mount Sinai, New York, NY

Abstract

Although the principles that balance stem cell self-renewal and differentiation in normal tissue homeostasis are beginning to emerge, it is still unclear whether cancer cells with tumor initiating potential are similarly governed, or whether they have acquired distinct mechanisms to sustain self-renewal and long-term tumor growth. Here we show that the transcription factor Sox2, which is not expressed in normal skin epithelium and is dispensable for epidermal homeostasis, marks tumor initiating cells (TICs) in cutaneous squamous cell carcinomas (SCC). We demonstrate that Sox2 is required for SCC growth in mouse and human, where it enhances Nrp1/Vegf signaling to promote the expansion of TICs along the tumor-stroma interface. Our findings suggest that distinct transcriptional programs govern self-renewal and long-term growth of TICs and normal skin epithelial stem and progenitor cells. These programs present promising diagnostic markers and targets for cancer specific therapies.

*To whom correspondence should be addressed Ronald O. Perelman Department of Dermatology, New York University School of Medicine, 522 First Avenue, Smilow Research Building. 411, New York, NY-10016, Markus.Schober@nyumc.org, Tel # 212-263-9251, Fax # 212-263-5819.

Author Contributions

J.S. and M.S. designed experiments. J.S., A.B., A.S.P, Y.Y., J.B, and R.S. performed the experiments. J.S., A.B., A.T., A.S.P, Y.Y., J.B, R.S. and M.S. analysed the data. J.A.C provided human SCC discard tissue and interpreted data. J.S., M.R., and M.S. wrote the paper. All authors provided intellectual input, read and approved the manuscript.

The authors declare no competing financial interests.

Accession codes

Differential gene expression analyzes between CSCs, EPI and HFSCs have been deposited at GSE29328.

Introduction

Identification of self-renewing cancer stem cells (CSCs), uniquely capable of sustaining long-term growth of hierarchically organized cancers[1], implies that cancer therapies that target and destroy CSCs may cure rather than just temporarily contain the disease[2]. The development of such CSC-specific therapies, however, depends on the identification of CSCs and the molecular mechanisms that are essential for their viability, self-renewal, and long-term tumor initiating potential, and at the same time dispensable for normal tissue stem cell functions.

Skin epithelium and cutaneous squamous cell carcinoma (SCC) present powerful model systems in which to investigate whether stemness is governed by the same or distinct molecular mechanisms in homeostasis and carcinogenesis. In skin epithelium a number of stem and progenitor cell populations have been identified[3–8]. Most prominent are hair follicle stem cells (HFSCs) that are located in the lower, permanent part of the hair follicle known as bulge. HFSCs have first been defined based on their slow-cycling behavior[9] and elevated colony forming potential[10], which enabled the identification of transcriptional[11,12] and epigenetic[13] signatures that distinguish HFSCs from other skin epithelial cell types. HFSCs have been isolated based on their expression of the cell surface proteins α6 and β1 integrin as well as CD34, cultured on 3T3 feeder layers long-term, and differentiated into all skin epithelial cell lineages upon transplantation onto *Nude* mice[14]. These properties defined HFSCs as stem cells and distinguished them from other skin epithelial cell lineages with limited proliferative potential[15].

Similarly, cutaneous SCC, a hierarchically organized skin cancer that can originate from HFSCs as well as other skin epithelial cells[16–18], is sustained by cancer cells with tumor initiating potential, which self-renew and also differentiate into tumor cells without the ability to form tumors upon transplantation[19]. Tumor initiating cells (TICs) in murine cutaneous SCC have been identified at the tumor-stroma interface where they express high levels of α6 and β1 integrin as well as CD34[20,21]. These cells are able to initiate and propagate SCCs that resemble the phenotypic heterogeneity of their parent in serial transplantation experiments. Differential gene expression analyses defined a characteristic molecular signature that distinguishes TICs in SCCs from normal skin epithelial stem and progenitor cells[20]. Intriguingly, essential HFSC regulators including Lim homeobox 2 (Lhx2), which maintains hair follicle stem cell function[22], T-box protein 1 (Tbx1), which governs their self-renewal[23], and nuclear factor of activated T cells 1 (Nfatc1), which restricts their activation[24] and functions as a tumor suppressor gene[25], are strongly repressed or undetectable in TICs of murine SCCs[20] (Fig.1a). This observation suggested the hypothesis that self-renewal and long-term growth of SCC initiating tumor cells may be governed by molecular mechanisms that are distinct from normal skin epithelial stem and progenitor cells from which the tumors originated.

Here we identify three transcription factors including SRY (sex determining region Y)-box 2 (Sox2), paired-like homeodomain transcription factor1 (Pitx1), and twist basic helix-loop-helix transcription factor 1 (Twist1), which are expressed in mouse and human SCCs, while they are not detectable in normal skin epithelial cells. We find Sox2 expressing SCC cells

within the α6 and β1 integrin expressing cell population lining the tumor-stroma interface. Sox2 expression is critical for tumor initiation and growth as it promotes the expansion of tumor initiating SCC cells along the tumor-stroma interface.

Results

Sox2 expression identifies TICs of cutaneous SCCs

To discover molecular markers unique to TICs, we directly compared global gene expression profiles of mouse epidermal SCC TICs with hair follicle stem cells (HFSCs) (Fig. 1a) and epidermal progenitor cells (Epi, Supplementary Fig. 1a)[20]. Among the molecules that are consistently expressed in all TIC populations, with expression tightly repressed in normal skin epithelial stem and progenitor cells, as well as in their differentiating progeny, are three transcription factors: Sox2, Pitx1, and Twist1 (Fig. 1a, Supplementary Fig.1). In contrast, the HFSC regulators Lhx2, Tbx1 and Nfatc1 are strongly repressed or undetectable in SCC TICs. The differential expression of these identified molecular markers was further confirmed by qRT-PCR analyses on freshly isolated TICs and HFSCs (Fig. 1b, Supplementary Fig. 2).

Next, we established primary cultures from TICs and HFSCs, which are able to proliferate over many passages *in vitro* reflecting their long-term self-renewing potential. We then evaluated the relative expression of our candidate genes in both cultures by qRT-PCR analyses. Expression of Sox2, Pitx1 and Twist1 was significantly elevated in cultured TICs compared to primary keratinocyte cultures established from HFSCs (Fig. 1c), while the HFSC self-renewal gene Tbx1[23], and the embryonic stem cell self-renewal genes and Sox2 partners Oct4 and Nanog[26], remained repressed in cultured TICs (Supplementary Fig. 3). We surmised that if Sox2, Pitx1 and Twist1 are indeed required for the self-renewing potential of TICs in SCC, then they should also be expressed in tumor initiating human SCC cell lines[27,28]. Indeed, qRT-PCR analyses confirmed the elevated expression of SOX2, PITX1 and TWIST1 in human SCC lines when compared to normal human keratinocyte cultures (Fig. 1d, Supplementary Fig. 4a). Furthermore, Western blot analyses for Sox2 also showed significant enrichment in both mouse and human SCC cultures when compared to normal keratinocyte cultures, confirming our results at the protein level (Fig. 1e–g, Supplementary Fig. 4b).

SOX2 expressing SCC cells reside at the tumor-stroma interface

To determine the location of Sox2 expressing cells in mouse and human tumor specimens, we analyzed their distribution by immunofluorescence microscopy and immunohistochemistry. Confirming our Sox2 expression analyses in sorted normal and tumor tissue cell fractions, Sox2 was not found by immunofluorescence in normal skin epithelium[29,30] but it was readily detected in murine tumors (Fig. 1h–k). In benign papillomas, Sox2 was expressed in a few undifferentiated tumor cells that reside at the tumor-stroma interface, but it was more readily observed within their differentiating progeny (Fig. 1h). In primary SCCs however, Sox2 expression was consistently detected (20/20) in nuclei of undifferentiated SCC cells, which clustered in areas at the tumor-stroma interface, where they express high levels of the basal cell markers α6 and β1 integrin (Fig. 1i).

Intriguingly, the focal localization of nuclear Sox2 expressing SCC cells was expanded to include the majority of undifferentiated tumor cells in secondary SCCs, which developed after transplantation of α6 and β1 integrin-expressing SCC cells onto *Nude* hosts (Fig. 1j). Likewise, nuclear Sox2 expression was also detected in the majority of undifferentiated keratin 14 positive cells in spontaneous lung metastases (5/5), which formed in less than 5% of our DMBA-treated mice (Fig. 1k, Supplementary Fig. 5).

A similar differential expression pattern was also observed in human skin and primary human SCCs (Fig. 1l–o, Supplementary Fig. 6). SOX2 expression was not detectable in normal human skin epithelium (Fig. 1l) but it was frequently found in clusters of undifferentiated tumor cells residing at the tumor-stroma interface of patient derived SCCs and in tumors grown after xenotransplantation of human SCC cell lines onto *Nude* mice (Fig.1m, n). Indeed, nuclear Sox2 expression was prevalent in 75% of patient derived SCCs, but it varied in expression levels and abundance between specimens (Fig. 1o, Supplementary Fig. 6). Together, the differential and prevalent expression of Sox2 in mouse and human cutaneous SCCs and its enrichment in TICs suggests Sox2 as a novel molecular marker that distinguishes TICs from normal skin epithelial stem and progenitor cells.

Epigenetic changes enable de novo Sox2 expression in SCC

A priori, this de novo expression of Sox2 in cutaneous SCCs could result from genetic as well as epigenetic changes. To test whether elevated Sox2 expression in SCC TICs compared to normal skin epithelial stem and progenitor cells is due to genomic amplification as recently reported for human esophageal and lung SCCs[31,32], we determined the copy number variation by TaqMan qRT-PCR assays. Our measurements revealed no genomic amplification of the Sox2 locus in mouse and human cutaneous SCC cultures (Supplementary Fig.7a). Indeed, Sox2 is expressed in normal esophageal stem and progenitor cells as well as lung epithelial cells during homeostasis[29], while Histone H3 lysine 27 trimethylation (H3K27me3) of the Sox2 promoter indicates transcriptional repression in skin epithelial stem and progenitor cells[13,33]. To test whether the de novo expression of Sox2 in cutaneous SCC TICs is due to a loss in H3K27me3, we determined whether the Sox2 promoter carries this repressive chromatin mark by ChIP-PCR. Our analysis revealed that the repressive H3K27me3 mark was significantly reduced in TIC compared to HFSC derived keratinocyte cultures consistent with the de novo expression of Sox2 (Supplementary Fig. 7b). Intriguingly, the reduction in H3K27me3 repression appears to be locus specific rather than genome-wide, because H3K27me3 levels were elevated at other gene promoters and on total protein extracts of SCC TIC compared to HFSC derived keratinocyte cultures (Supplementary Fig. 7b–c). Furthermore, Polycomb Repressive Complex components were expressed in both TICs of cutaneous SCCs and normal skin epithelial stem and progenitor cells (Supplementary Fig 7d).

SOX2 promotes SCC initiation and growth

To test whether SOX2 expression is required for SCC growth, we infected human SCC lines and primary murine TICs with lentivirus expressing histone 2B - red fluorescent protein (H2B-RFP) along with a short hairpin RNA (shRNA) that efficiently reduced SOX2 mRNA and protein levels (Supplementary Fig. 8a–c). Lentivirus expressing Scrambled (SCR)

shRNA along with histone 2B - green fluorescent protein (H2B-GFP) was used as control[34]. Control (shSCR) and SOX2 knockdown (shSOX2) cells were transplanted onto *Nude* recipient mice, where control infected tumors grew rapidly and at a similar rate to uninfected SCCs, while SOX2 depletion resulted in delayed and significantly reduced SCC growth (Fig. 2a, Supplementary Fig. 8d). Intriguingly, only (8/16) tumors initiated following transplantation and 2 of these tumors regressed after initial signs of tumor growth.

The severe reduction in tumor growth following SOX2 depletion suggested a critical role for SOX2 in tumor initiation and/or maintenance. To address if SOX2 function is still required once SCCs are established, we transplanted human and mouse TICs infected with a lentivirus encoding a doxycycline-regulated shSOX2 onto *Nude* mice. Induction of shSOX2 in fully formed tumors resulted in a significant reduction in growth of both human (Fig. 2b) and murine (Supplementary Fig. 8e) SCC grafts.

To investigate the cellular defects responsible for the reduced tumor growth, we measured the relative rates of proliferation and apoptosis in control and SOX2 depleted SCC grafts. SCC sections were stained with the proliferation markers Ki67 (Fig.2c) and phospho-histone H3-Ser10 (Fig.2d), as well as active Caspase 3 (Fig.2e) to detect apoptotic cells within the H2BGFP or H2BRFP labeled tumor epithelium. shSOX2 knock-down SCCs showed a small but significant decrease in proliferative tumor epithelial cells and a significant increase in apoptotic figures.

We surmised that SOX2 could promote SCC growth by cell intrinsic as well as extrinsic mechanisms. To test this hypothesis, we performed clonal competition and lineage trace studies in our human (Fig. 2f–g) and mouse (Supplementary Fig. 8f–g) SCC transplantation models. We produced a mixture of control (shSCR-GFP) and knockdown (shSOX2-RFP) lentivirus, and infected TICs at clonal density, so that only a small percentage of cells were transduced. To ensure that equal GFP/RFP numbers of sparsely transduced cells were transplanted, we measured the transduction efficiency by flow cytometry prior to their injection into *Nude* recipient mice. We then allowed the transplants to develop into tumors, which we processed to directly compare the growth characteristics of SOX2-positive and SOX2-negative clones within the same tumor. Interestingly, clone size measurements revealed no significant differences between control and SOX2 knockdown clones within the first 2 weeks of tumor growth (Fig. 2f–g and Supplementary Fig. 8f–g). However, 4 weeks following transplantation, SOX2-depleted clones were significantly smaller when compared to control ($P<0.0001$; Fig. 2f–g and Supplementary Fig. 8f–g). In addition to quantitative immunofluorescence microscopy of transduced SCC clones, we performed a series of flow cytometric analyses, measuring the ratios of Sox2-depleted and control cells in SCCs over time. These experiments confirmed that, although the ratio of Sox2 negative/positive cells remains unchanged during the initial growth period, Sox2 knockdown cells are eventually outcompeted by Sox2-positive cells (Supplementary Fig. 8h). Similar results were obtained in clonal competition experiments in culture (Supplementary Fig. 8i).

The severe reduction in SCC growth following Sox2 knockdown indicated an essential function in SCC initiation and maintenance. To test whether ectopic Sox2 expression is sufficient to initiate and drive SCC growth, we infected primary HFSC derived keratinocyte

cultures with lentivirus expressing Sox2 under the ubiquitous PGK promoter followed by their transplantation into Nude mice. Keratinocytes infected with LZRS-Ras^{G12V} were used as a positive control. In contrast to LZRS-Ras^{G12V} infected HFSCs, which formed tumors efficiently following transplantation into Nude mice[35], ectopic expression of Sox2 alone was not sufficient to initiate skin carcinogenesis (Supplementary Fig. 8j). Together, our data indicate that Sox2 is critical for SCC growth, but insufficient to initiate skin carcinogenesis.

To better understand how Sox2 promotes SCC growth at the molecular level, we compared the gene expression signature that distinguishes TICs from normal skin epithelial stem and progenitor cells[20] (Fig.1a) with direct Sox2 target genes in embryonic stem cells[36]. This analysis identified 466 putative Sox2 targets (Fig. 3a, Supplementary Data 1), including the transcription factor Pitx1 and the pro-angiogenic factors Neuropilin (Nrp1, Nrp2)[37], Secreted Phosphoprotein 1 (Spp1)[38], Phosphatidylinositol transfer protein cytoplasmic 1 (Pitpnc1)[39], and Insulin growth factor 2 binding protein 2 (Igf2bp2), as genes with the highest differential expression in SCC TICs (Fig. 3b–c). To establish whether their expression is dependent on Sox2 function, we first verified their elevated expression in TICs compared to HFSCs by qRT-PCR (Fig. 3d). We then measured their expression in Sox2 knockdown TICs compared to Scr controls. Indeed, all of our candidate genes were detected at significantly lower expression levels when Sox2 was depleted - consistent with a function for Sox2 in regulating their expression in TICs (Fig. 3e). In addition, we performed chromatin immuno-precipitation (ChIP) PCR experiments, and demonstrated a significant enrichment of Sox2 protein at the enhancer sequences of these genes (Fig. 3f). Notably, Sox2 also promoted the expression of Vegfa and the epidermal growth factor receptor (EGFR) ligands Epiregulin (Ereg) and Tumor growth factor alpha (Tgfα), which are contained in our list of signature genes that are expressed in TICs but not in HFSCs (Fig. 3g–h).

Elevated expression levels of Vegfa and Nrp1 suggested that Sox2-positive cells might be located in close proximity to tumor endothelial cells as previously reported for CD34-positive TICs, which express elevated levels of Nrp1, Vegfa, as well as Sox2[40]. To test this hypothesis, we measured the closest distance between basal SCC cells with high SOX2 expression and CD31-positive tumor endothelial cells by quantitative immunofluorescence microscopy. Our measurements revealed that SCC cells, which are located at the tumor-stroma interface and express high levels of SOX2, are often found in clusters located in close proximity to CD31-expressing tumor endothelial cells (Fig.3i–j).

SOX2 controls NRP1 expression and SCC growth

Nrp1/Vegfa signaling is critical for tumor growth in murine SCC where it promotes cell proliferation, survival and symmetric self-renewal[40,41]. To investigate whether NRP1 expression is dependent on SOX2 function in human SCC, we first measured the relative expression levels of NRP1 in control and SOX2 depleted human SCC cells. qRT-PCR revealed significantly reduced NRP1 expression in shSOX2 depleted human SCC cells compared to controls (Fig.4a). In addition, SOX2 was significantly enriched at the NRP1 locus as measured by quantitative ChIP-PCR analyses (Fig. 4b). These data together with

Nrp1's previously described role in murine SCCs, suggested NRP1 as one possible molecular target responsible for SCC initiation and growth in human SCCs.

To test whether NRP1 function is critical to skin carcinogenesis in human, we first compared the growth kinetics of shSCR-GFP and shNRP1-RFP in our xenotransplantation model. Similar to SOX2, NRP1 depletion resulted in 40% reduced SCC initiation, spontaneous regression of one tumor, and significantly delayed growth kinetics of the remaining transplants (Fig. 4c). Consistent with the slower tumor growth we measured significantly reduced proliferation (Fig. 4d–e), while apoptosis rates were comparable between shNRP1 and shSCR expressing tumors (Fig. 4f). Likewise, quantitative lineage trace analyses of clonally transduced human SCCs revealed no significant differences in the initial growth followed by the depletion of shNRP1-RFP knockdown clones compared to shSCR-GFP controls, mirroring the growth behavior of SOX2 depleted SCC cells (Fig. 4g, h).

Intriguingly, flow cytometric analyses of our clonal competition experiments revealed a subtle decrease in the relative number of NRP1 depleted SCC cells expressing high levels of α6 integrin, while the population of NRP1 deficient cells expressing low levels of α6 integrin was significantly increased (Fig. 4i). These data suggest that NRP1 depleted clones might also differentiate more rapidly than scrambled controls within the same tumor. This observation is consistent with previous reports where Nrp1 functions to promote self-renewing cell divisions along the tumor-stroma interface in murine SCCs[40]. To test if this function of Nrp1 is conserved in human SCCs we stained our xenografts with the spindle mid-body marker Survivin and the extracellular matrix marker Nidogen and measured the orientation of cell divisions relative to the tumor-stroma interface of test (shNRP1-RFP) and control (shSCR-GFP) cells within the same tumor. Control basal SCC cells divided predominantly along the tumor-stroma interface, while the orientation of NRP1 depleted basal SCC cell divisions appeared randomized (Fig. 4j).

Given the direct links between SOX2 and NRP1 expression we wondered whether SOX2 expression correlates with oriented cell divisions along the tumor-stroma interface. We first stained human SCC xenografts with the spindle mid-body marker Survivin and measured the orientation of basal, SOX2-positive and SOX2-negative cell divisions in late mitosis. We observed that SOX2-positive cells divided predominantly parallel to the basement membrane, whereas the division axis of the rare, SOX2-negative basal SCC cells was randomized (Fig. 5a, b). A similar distribution was observed in primary mouse SCCs where Sox2-negative cells are more common (Fig. 5c). To functionally probe this correlation and test whether SOX2 is indeed required to direct the orientation of basal SCC cells, we measured the division axis in shSCR-GFP control and shSOX2-RFP knockdown clones in respect to the tumor-stroma interface. Our measurements revealed that basal cells within control clones divided primarily in parallel to their underlying stroma, whereas the division axis in basal SOX2 knockdown cells was randomized in both human (Fig. 5d, e) and mouse (Fig. 5f) SCC grafts. These results support the hypothesis that Sox2 expression biases TICs to divide along the tumor-stroma interface thereby expanding the undifferentiated and proliferative tumor fraction/compartment.

Indeed, we counted significantly fewer undifferentiated, α6 and β1 integrin-expressing cancer cells in Sox2-depleted clones when compared to Scr controls (Supplementary Fig. 8k). In addition, sensitive flow cytometry assays corroborated this observation, as they detected a small reduction in the relative portion of undifferentiated α6-high SCC cells and a significant increase in post mitotic, differentiating α6-low SCC cells even at two weeks after transplantation, when no significant differences in total clone size were detected (Fig. 5g–h). Together, these data suggest that Sox2 enhances TIC self-renewal and suppresses their differentiation, thereby promoting geometric growth within SCCs[42].

Discussion

Our study on cutaneous SCC, a paradigm for hierarchically organized cancers, provides important insights about the regulation of cancer cells with tumor initiating potential and their consequences for tumor growth. Cutaneous SCCs are, similar to normal skin epithelium, sustained by stem cells that self-renew and differentiate into progeny without long-term proliferative potential[42]. Although, TICs and normal skin epithelial stem and progenitor cells share some similarities including: their close association with the underlying stroma; their elevated expression of cell surface markers α6 integrin, β1 integrin, and CD34; their clonogenic potential in culture; and their regenerative capacity in vivo, our differential gene expression analyses identified a gene expression signature that distinguishes TICs from HFSCs[14,20,21,43]. Surprisingly, transcription factors that specify HFSC and sustain their long-term self-renewing potential are not detected in TICs of SCC. Instead, a tumor specific transcriptional program, not expressed in normal skin epithelial cells, becomes established de novo as SCCs initiate and progress (Fig. 1). This program, which specifies TICs and distinguishes them from normal skin epithelial stem and progenitor cells both molecularly and functionally, is expressed in both mouse and human SCCs.

As part of this tumor specific transcriptional program, we discovered Sox2 as a novel, functional marker for TICs in mouse and human SCCs. While tightly repressed in normal skin epithelium and dispensable for skin epithelial homeostasis, Sox2 activity is critical for tumor initiation, maintenance, and SCC growth in mouse and human. The expression of Sox2 during the course of carcinogenesis correlates with a loss of the repressive H3K27me3 chromatin mark at the Sox2 promoter, while its copy number was unaffected (Supplementary Fig. 5). Intriguingly, the reduction of H3K27me3 appears to be locus specific rather than global as Polycomb Repressive Complex complex components are expressed and active. Although the molecular mechanisms leading to the de-repression of Sox2 remain to be identified in cutaneous SCCs, a similar locus specific de-repression resulting in de novo Sox2 expression in synovial sarcoma had been linked to the disruption of mSWI/SNF (BAF) complexes[44].

Once expressed, Sox2 becomes essential for SCC growth and maintenance. Our findings therefore suggest the feasibility of therapies that directly aim at cancer cells with tumor initiating potential, while leaving normal stem and progenitor cells unaffected. The successful development of such therapies, however, will require a comprehensive understanding of the circuitry that enables and sustains Sox2 expression in TICs of SCC, in addition to the identification of lineage-specific transcription factors that partner with Sox2

to sustain its activity in SCC TICs. While our current study focuses on a subset of Sox2 target genes that are common between TICs in SCC and embryonic stem cells (ESCs), it remains to be defined how Sox2 regulates the expression of these genes. This is important because the Sox2 partners Oct4 and Nanog, which are critical for its function in ESCs, are not expressed in SCC TICs (Supplementary Fig.3)[20]. Indeed, several novel Sox2 binding partners have been identified in human head and neck SCCs[45], directing Sox2 activity to numerous genomic loci, where it can function as both a transcriptional activator as well as a repressor[46].

Nrp1 has surfaced together with several other pro-angiogenic factors as direct Sox2 target genes with the highest differential expression between TICs and skin epithelial stem and progenitor cells. Importantly, Nrp1 was not only a Sox2 target in mouse but also in human. In addition to Nrp1, Vegfa and the Egf-receptor ligands Tgfα and Ereg are also highly expressed in TICs, while they are not detected in HFSCs (Supplementary Fig. 1c). Our data therefore suggest a critical role for Sox2 in promoting a synergistic auto-regulatory feedback loop between Nrp1/Vegf and Egfr signaling, which promotes proliferation and cell survival to drive rapid SCC growth[40,41,47]. Combined inhibition of Egfr and Vegf signaling in skin epithelial cells prevents the initiation of skin tumors[41]. Consistent with this report we find a 50% reduction in the tumor initiating potential of Sox2 depleted tumors. Intriguingly, the shSox2-RFP transduced tumors, which did initiate, were often comprised of both transduced and un-transduced SCC cells, suggesting the possibility that growth factors secreted from Sox2-positive tumor epithelial cells may have supported the growth of Sox2-depleted tumor cells. Nevertheless, proliferation rates were significantly reduced as previously reported for SCCs where Nrp1/Vegf signaling was compromised[40,41] and apoptosis rates were significantly increased consistent with compromised Egfr signaling in SCCs[47].

Interestingly, Sox2 depletion in single cell clones also affected the rate of tumor cell clone size expansion in human and mouse, indicating that Sox2-positive clones expand geometrically, whereas SOX2 knockdown clones appeared to expand via linear growth kinetics (Fig 2f–g, Supplementary Fig. 8f–g). A similar result was obtained in human SCCs, when NRP1 was depleted at the clonal level (Fig. 4g–h). This growth difference could be simply explained by the reduced proliferation and apoptosis rates. However, it is intriguing to speculate that SOX2 or NRP1 depleted TICs could change the mode rather than the rate of cell division. In normal epidermis, the progenitor cell pool can expand by symmetric cell divisions in the basal layer that are parallel in respect to their underlying basement membrane, while perpendicular divisions enable an asymmetric lineage choice, which maintains an uncommitted and proliferative basal daughter cell, in addition to an apical daughter that commits to squamous differentiation[48,49]. Indeed, symmetric and asymmetric cell divisions have also been described in basal cells of murine SCCs, where the division axis was dependent on Nrp1 function[40]. In analogy to these studies, we observed differences in the orientation of dividing SOX2 positive and SOX2 negative SCC cells with respect to the tumor-stroma interface. Although our data support the hypothesis that SOX2 and NRP1 promote the division and expansion of TICs along the tumor-stroma interface to expand the proliferative SCC cell pool, further studies including the reconstruction and measurement of TIC divisions in three dimensions and the identification of cell fate determinants, which differentially segregate between daughter cells upon cytokinesis, are required before the

divisions can be defined as either symmetric or asymmetric. To date, mechanisms controlling self-renewal and differentiation are only beginning to emerge. Still, the mode by which TICs divide may be critical for therapy resistance and therapy design[50]. Therefore, our observation that division orientation and geometric expansion in clonal trace experiments depend on SOX2/NRP1 function in both mouse and human SCCs provide a starting point to further investigate the links between cell division and differentiation in skin carcinogenesis.

Taken together, our data suggest that Sox2 functions as a pivotal molecule in SCCs as it acts as an integration point of developmental and oncogenic signaling mechanisms. Sox2 expression not only renders TICs self-sufficient for essential mitogenic stimuli, it also provides critical pro-angiogenic cues that ensure the blood supply and waste disposal for a rapidly expanding tumor – thereby affecting several hallmarks of cancer[51].

Methods

Constructs and RNAi

All shRNAs were obtained from the Mission TRC-1 mouse and human library (Sigma), cloned into pLKO.1 (Addgene 8453), and subsequently cloned into pLKO Histone H2B-mRFP1 (Addgene 26001) or pLKO Histone H2B-GFP (Addgene 25999)[34] or cloned directly into pLKO Tet-on puro (Addgene 21915)[52].

pLKO-no stuffer-PGK-mSox2-3X Flag was generated as follows: 1) mSox2 was amplified by PCR from FU-CRW-mSox2-RFP using primers 5’-atgcatAAGCTTgtatggtcccgggggcagcg-3’ and 5’-atgcatAGATCTtcacatgtgcgacaggggca-3’, and then digested with HindIII and BglII. The PCR product was ligated with 3XFLAG-CMV10, digested with HindIII and BglII, to generate 3xFlag-mSox2-CMV10. 2) mSox2 was PCR amplified from 3xFlag-mSox2-CMV10 using primers 5’-atgcatACCGGTaccatggtatggtcccgggggca-3’ and 5’-atgcatCTCGAGcatgtgcgacaggggcagtg-3’, and then the PCR product and PQCXIX-MCS-3xFlag-IRES-tomato were digested with AgeI and XhoI and ligated to generate PQCXIX-mSox2-3xFlag-IRES-tomato. 3) PQCXIX-mSox2-3xFlag-IRES-tomato and pLKO no stuffer PGK MCS were digested with BamHI and BlpI, and mSox2-3xFlag was subcloned into pLKO no stuffer-PGK-MCS to generate pLKO-no stuffer-PGK-mSox2-3X Flag.

The following shRNAs were used: shScramble (SHC002), shSox2 (TRCN0000424718, TRCN0000085748, TRCN0000231643, and TRCN0000257314) and shNRP1 (TRCN0000322980). For full hairpin sequences see Supplementary Table 1.

Cell culture

All primary cell lines were maintained as previously described[53,54] except for human squamous cell line SCC-13, which was grown in 1.5 μM calcium (high calcium medium) and human cell line A431, which was grown in DMEM with 10% FBS. Human head and neck squamous cell carcinoma cell lines were cultured in P medium (DMEM:F12 [3:1], sodium bicarbonate [Sigma], L-glutamine [Invitrogen] and Pen/Strep solution [Invitrogen])

with 10% FBS). Human cell lines were obtained from ATCC (A431) or Harvard Skin Disease Research Center Cell Culture Core[27], and primary murine cell lines were tested for mycoplasma contamination (mouse essential virus panel, Charles River Research Animal Diagnostic Services).

For stable cell line generation, lentivirus was produced by Lipofectamine 2000 (Invitrogen) transfection of 293FT cells (Invitrogen) with pLKO shRNA-carrying plasmid and helper plasmids pMD2.G and psPAX2 (Addgene plasmid 12259 and 12260, respectively). 293FT cells were maintained in media consisting of 75% D10 media (DMEM [Gibco], 0.075% sodium bicarbonate, 1% L-glutamine and Pen/Strep solution [Invitrogen], 10% FBS, 1mM sodium pyruvate [Invitrogen]) and 25% OptiMem Mix (Opti-MEM [Invitrogen] and 10% FBS). Viral supernatant was collected 36h and 60h after transfection and filtered through a 0.22μm filter. For viral infections, 10,000 cells were plated per well in 6-well plate, and incubated with lentiviral supernatant in the presence of 31 μg/mL of polybrene and spun at 1,100×g for 30min at 37°C.

Infected cells were FACS-sorted 60hr post-infection and used in analyses of in vivo tumor growth (whole tumor and clonal competition), and in vitro clonal competition. For tumor growth assays, FACS isolations were performed on a BD FACSAria II equipped with 488, 633, 405, 562 and 355nm lasers. Cells were gated on live, single cells, and sorted for either GFP+ or RFP+ (shRNA-carrying) cell populations. Sorted cells were suspended in 50% Matrigel (356237; BD) diluted with F medium at a concentration of 10,000 (murine) or 50,000–100,000 (human) cells per injection and injected intradermally into Nude (NU/NU [088] Charles River) recipient mice. For clonal competition assays, both viruses (Scr-GFP and Sox2-RFP) were produced in the same well by using equal amounts of each shRNA-carrying plasmid. Infected cells were analyzed prior to injection to determine RFP/GFP ratios using a BD LSR II.

Antibodies, immunohistochemistry and imaging

Unfixed tumors were embedded in OCT (Tissue Tek). Frozen sections were cut to a thickness of 12–30μm on a Leica cryostat and mounted on SuperFrost Plus slides (Fisher). Slides were air-dried for 10min, then fixed for 5–10min with 4% formaldehyde (28908, Thermo Scientific), rinsed with PBS, permeabilized with 0.1% Triton X-100 in PBS for 15min, then blocked for 1h in gelatin block (5% normal donkey serum, 1% BSA, 2% gelatin, 0.2% Triton X-100 in PBS) or NDS/NGS block (5% normal donkey serum, 5% normal goat serum, 0.2% Triton X-100 in PBS), and incubated in primary antibody diluted in blocking buffer at 4°C overnight. After washing with PBS, secondary antibodies, conjugated to Alexa 488, FITC, Alexa 568, DyLight 649, DyLight 405 and Hoechst 33342 (83218, AnaSpec) were diluted in blocking buffer and incubated with the slides for 1h at room temperature. After washing, slides were mounted in ProLong Gold (Invitrogen) or Vectashield (H-1400, Vector Laboratories). Imaging was performed on a Nikon Eclipse TiE Microscope, Leica TCS SP5 II Confocal Microscope, Zeiss LSM510 Confocal Microscope or Zeiss LSM780 Confocal Microscope. Image stacks were visualized in Volocity 6.0. For Survivin and Sox2 co-stainings on primary mouse and human xenograft SCC tumors, the same protocol was followed except for the following: sections were incubated overnight

with rabbit anti-Sox2, washed, stained with secondary anti-rabbit Alexa 488, washed, and incubated with rabbit anti-survivin and rat anti-CD104/ β4 (mouse samples only) or rat anti-CD49f/ α6-PerCP-Cy5.5 (human samples only) overnight, washed and, incubated with secondary anti-rabbit Alexa 568, anti-rat DyLight 649 and Hoechst, washed and mounted in ProLong Gold. For detailed list of antibodies and dilutions see Supplementary Table 2.

Human tissue microarray and paraffin SCC & metastases stainings

Primary human SCC specimens have been de-identified and supplied by NYU's tissue acquisition and banking service. Human skin squamous cancer tissue microarray (SK802a, US Biomax) was dewaxed and hydrated (2x Xylene, 2× 100% EtOH, 2× 95% EtOH, 1× 70% EtOH and 1× 50% EtOH for 3min each). After rinsing in PBS, slides were placed into a water bath (98°C for 20min) in sodium citrate buffer (10mM sodium citrate, pH 6.0) for heat-induced antigen retrieval. Endogenous peroxidase activity was blocked using BloxALL (SP-6000, Vector Laboratories) for 10min at room temperature (RT) after wash in PBS. Following washing, slides were blocked in NHS block (0.3% Triton X-100, 1% BSA, 5% normal horse serum in PBS) for 30min at RT. Primary antibody was diluted in NHS blocking buffer and slides incubated at 4°C overnight. Slides were washed with 0.3% Triton X-100 in PBS and incubated with biotinylated secondary anti-rabbit IgG (H+L) for 30min at RT. After final washes, slides were incubated with ABC solution (PK-4000, Vector Laboratories) for 30min at RT. Following washes, staining was developed by incubating with ImmPACT DAB (SK-4105, Vector Laboratories) for 2–10min at RT. Reaction was stopped by washing with ddH_2O. Slides were dehydrated (1× 50% EtOH, 1× 70% EtOH, 1× 95% EtOH, 2× 100% EtOH and 2x Xylene for 3min each) and mounted with Permount (SP-15-100, Fisher Scientific). A detailed list of antibodies and their working concentrations can be found in Supplementary Table 2.

Genomic meta analyses

Differential gene expression analyzes between CSCs, EPI and HFSCs (GSE29328) has been analyzed in Gene Pattern software as previously described[20]. Average expression values across 16 independent CSC populations and replicate HFSC or EPI populations has been computed in MATLAB and presented as scatter plots. Transcription factors with the highest differential expression values in CSCs and HFSCs have been indicated as red and green dots respectively. Pre-computed Sox2 peaks obtained from GEO repository accession number GSE11431 (series GSM288347) were converted from assembly version mm8 to assembly version mm10 using UCSC Genome Browser liftover utility[55]and used for our analyses. Read alignments to human assembly version hg18 were downloaded from GEO (accession series GSM456570) and peaks were computed using MACS[56] version 1.4 with default parameters except for using a fragmentation size of 400bp. Peaks were then converted to human assembly version hg19 using UCSC Genome Browser liftover utility.

qRT-PCR

For culture experiments, cells were grown at 4%O_2,7% CO_2 and serum-starved 24h before harvesting. mRNA was isolated using Qiazol (Qiagen) and Direct-zol RNA Mini Prep (R2052, Zymo Research), or Absolutely RNA Nanoprep Kit (400753, Agilent Technologies). Samples were quantified using a Nanodrop spectrophotometer (Thermo

Scientific). cDNA was synthesized from 300 ng to 1.5 μg of total RNA using SuperScript VILO with random primers (Invitrogen) or SuperScript III First-Strand Synthesis System (Invitrogen) with oligo(dT) primers. Quantitative real-time PCR (qRT-PCR) was performed with Absolute Blue QPCR SYBR Green Mix plus ROX Vial Kit (AB-4166, Thermo Scientific) on a MyiQ2 (BioRad), or with LightCycler DNA Master SYBR Green I reagents (Roche) on a Light Cycler 480 (Roche). Measurements were recorded in duplicate or triplicate. Differences between samples and controls were calculated based on the $2^{-\Delta\Delta CT}$ method and normalized to Rplp0 (mouse) or RPLP0 (human). For detailed list of primer sequences see Supplementary Table 3.

ChIP-PCR

For chromatin immunoprecipitation, cells were grown at 4%O_2, 7% CO_2 and serum-starved 24h before harvesting. Cells were fixed in fixation buffer (1% formaldehyde, 10mM HEPES pH7.6, P low calcium media [50 μM calcium, DMEM:F12 {3:1} without calcium] [Special order, Gibco cat#90-5010EA], sodium bicarbonate, L-glutamine and Pen/Strep solution), lysed using a series of lysis buffers (lysis buffer I [50mM HEPES pH7.6, 140mM NaCl, 1mM EDTA, 10% Glycerol, 0.5% NP-40 and 0.25% Triton-X 100 in ddH_2O], lysis buffer II [10mM Tris-HCl pH8.0, 200mM NaCl, 1mM EDTA and 0.5mM EGTA in ddH_2O] and lysis buffer III [10mM Tris-HCl pH8.0, 1mM EDTA, 0.5mM EGTA and 0.5% N-Lauryl Sarcosine in ddH_2O]) with cOmplete, Mini, EDTA-free protease inhibitor tablets (04693159001, Roche). Chromatin was sonicated to 200–500 base pair fragments using a Diagenode Bioruptor (Diagenode) employing a 30sec on/off regime.

For Sox2 ChIP experiments on mouse and human SCC cell extracts, chromatin immunoprecipitation was performed according to manufacturer's instructions using the EZ-Magna ChIP kit (Millipore). Chromatin (40 or 80 μg per IP) was immunoprecipitated with 2 or 4 μg mouse monoclonal anti-Sox2 antibody (17–656, Millipore) or control normal mouse IgG (17–656, Millipore) at 4°C overnight.

For H3K27me3 ChIP experiments, chromatin immunoprecipitation was performed using 10^6 cells per IP with 25 μl Dynabeads Magnetic Protein G (12321D, Invitrogen), and 5 μg anti-H3K27me3 (ab6002, Abcam) or control normal mouse IgG/IgG2b (sc-2025, Santa Cruz).

qRT-PCR was performed with the Absolute Blue QPCR SYBR Green Mix plus ROX Vial Kit (AB-4166, Thermo Scientific) on a MyiQ2 (BioRad), or FastStart Universal SYBR Green Master Mix (4913914001, Roche) on a StepOnePlus (Life technologies). Relative binding was calculated with the $2^{-\Delta\Delta CT}$ method and normalized to input. For detailed primer sequences see Supplementary Table 4.

SOX2 copy gene number

Genomic DNA was isolated using DNeasy Blood & Tissue Kit (69504,Qiagen). SOX2/Sox2 copy number was analyzed using the TaqMan copy number assay from Applied Biosystems (kit 4371355) and the TaqMan probe Hs 02753059 or Mn00549969. SOX2/Sox2 copy number was calculated relative to TERT/RNaseP or Tert/Tfrc expression, using the CopyCaller Software v2.0 from Applied Biosystems.

Western blotting

Cell lysates were prepared using RIPA buffer (150mM sodium chloride, 0.1% Triton-X 100, 0.5% sodium dodecyl sulphate and 50mM Tris pH8 in ddH_2O) with complete Mini EDTA-free protease inhibitor tablets (04693159001, Roche). Protein concentrations were determined following the instructions of Pierce BCA Protein Assay Kit (23225, Pierce). Lysates were boiled with 3x Laemmli buffer (6% SDS, 15% β-mercaptoethanol, 30% glycerol, 0.006% bromophenol blue, 0.188M Tris- HCl) for 10min at 95°C. Protein ladder used was Full-Range Rainbow Molecular Weight Markers (RPN800, GE healthcare). For murine samples, 30 μg of protein was loaded per lane. For human samples, 10–120 μg of protein was loaded per lane. Gel electrophoresis was performed using a 10 or 12% Bis-Tris gel run for 75–150min at 120V, gel was transferred for 1h at 4°C at 100V to a 0.45 μm nitrocellulose membrane (Whatmann) and transfer was assessed by Ponceau S staining (0.1% (w/v) Ponceau S in 5% (v/v) acetic acid). Membranes were blocked with 5% Nonfat Dry Milk in TBST, then incubated with primary antibodies diluted in blocking buffer or antibody dilutent (5% [w/v] BSA in TBST [TBS with 0.1 % Tween-20]) overnight at 4°C with gentle agitation. Membranes were rinsed with TBST before incubating with HRP-conjugated secondary antibodies diluted in blocking buffer for 1h at room temperature. Membranes were washed with TBST, then with TBS before incubating with the Luminata Classico or Crescendo Western HRP Substrate (WBLUC0500 or WBLUR0500, Millipore) and exposed to x-ray film (F-9024-8X10, GeneMate) using a Kodak X-Omat 2000A Processor. For detailed list of antibodies and dilutions see Supplementary Table 2. Full scans of Western blot films are provided in Supplementary Figure. 9.

Tumor isolation and flow cytometry

Tumors from murine allografts and human xenografts were isolated as previously described[20]. Briefly, after separating tumors from normal skin, blood vessels and connective tissue, tumors were minced and incubated with 0.25% collagenase (C2670, Sigma) in HBSS (Gibco) for 60 min at 37°C shaking. During the last 10 min of collagenase digestion, 62.5U/mL DNaseI (LS002138, Worthington) was added. The cell suspension was filtered through 70 and 40 μm cell strainer, where tissue remaining in filters was digested an additional 10 min with 0.25% trypsin (Invitrogen) at 37°C shaking and strained again. Cell suspensions were diluted in wash buffer (2% chelexed FBS in DPBS) and pelleted at 300×g for 10min. For human foreskin isolations, fat layer was removed from samples and incubated with the dermis-side down, in dispase (354235, BD Biosciences) overnight at 4°C. Epidermis was physically separated from the dermis, and rinsed in PBS followed by a 10 min incubation in trypsin at 37°C. Tissue was dissociated and filtered through a 70 and 40 μm cell strainer. Isolated cells were plated on 3T3 feeder cell layer in E medium with 15% Ca^{2+}-free FBS, 300μM calcium and Antibiotic-Antimycotic (15240112, Invitrogen). For flow cytometry, cell suspensions were stained for 30min on ice (for a detailed list of antibodies and dilutions see Supplementary Table 2) and DAPI (D1306, Invitrogen) was used for live/dead cell exclusion. FACS analyses were performed on a BD LSRII equipped with 488, 642, 407, 355 and 562nm lasers. Flow cytometry data analysis was carried out using FlowJo. For pre-injection clonal competitions, RFP+ and GFP+ cell populations were gated on live, single cells. For post-injection clonal competitions, RFP+ or GFP+ integrin^{hi}

and integrin^{low} cell populations were gated on live, single, RFP+ or GFP+ cells (lineage marker) followed by $\alpha6^{hi}$ $\beta1^{hi}$ (basal) and $\alpha6^{low}$ $\beta1^{low}$ (suprabasal) cells.

Epidermal stem and progenitor populations and hair follicle stem cells were sorted from single, live (DAPI), lineage positive (K14-H2BGFP)[11], CD49f-positive cells as the Sca1- and CD34-positive cell populations, respectively. Dermal papillae cells were isolated from single, live (DAPI), lineage positive (Lef1-RFP[57] and Itga9-positive cell populations[58].

Mice

Female 6-week old *Nude* (NU/NU [088] Charles River) mice were used for orthotypic transplantations and xenograft studies. Tumors were detected by palpation, measured using a digital caliper, and tumor volume was calculated ($V_{Tumor} = \frac{\pi}{6} x|x w^2$, where l=length in mm and w=width in mm). Mice were injected i.p. with 5-bromo-2′-deoxyuridine (BrdU) (Invitrogen 5 μl/mg of weight) 8h before sacrificing. For inducible RNAi-mediated knockdown in vivo, mice were placed on doxycycline-containing (200mg) diet after tumors were established, while control mice remained on a normal diet. Tumor volumes were calculated at the time mice where placed on doxycycline and this volume served as the baseline to calculate the fold change of tumor volume over time in treated and control mice.

All animal experiments were performed in accordance with the guidelines and approval of the Institutional Animal Care and Use Committee at New York University Langone Medical Center.

Measurements, quantification, graphing and statistics

All experiments were carried out single-blinded except for quantification of division axis in Sox2/SOX2 high and low cells, and assessment of SOX2 expression in patient SCC tissue microarrays, which were double-blinded. All RNAi-mediated knockdown experiments in vivo and in vitro were repeated three independent times with biological replicates. All quantitative data were collected from experiments performed in at least triplicate, and expressed as mean ± s.d., 95%CI, min/max or s.e.m. Differences between groups were assayed using unpaired or paired two-tailed student t-test, or Mann-Whitney test (proliferation and apoptosis quantifications, clonal size distributions and division axis) using Prism 6 (GraphPad Software). Box-and-whisker plots are used to describe the entire population without assumptions about the statistical distribution. Significant differences were considered when $P < .05$ as indicated by asterisks. For clonal competition assays, population sizes were determined by counting RFP+ or GFP+ cells. Integrin-high clones were defined as at least one RFP+ or GFP+ cell was located at the tumor-stroma interface (as indicated by CD104/ β4 or CD49f/ α6 staining) per clone. For proliferation and apoptosis quantifications, pictures were acquired at 20× magnification and deconvolved, before Ki67, pH3 or active Casp-3 expression was automatically detected in cells expressing either H2B-GFP (shSCR tumors) or H2B-RFP (shSOX2 or shNRP1 tumors) using the NIS element software. The percentage of Ki67, pH3 or active Casp-3 positive cells within the lineage was measured in more than 200 fields per condition and plotted in Prism 6. For quantification of division axis, the number of cells analyzed (n) is indicated in the radial histograms, and included cells from three or more tumors. Axis of division was determined as previously

described[49]. Briefly, staining for anaphase/telophase marker Survivin, which localizes to the spindle mid-body, is present at the mid-zone between two daughter nuclei. Angle of division was determined by measuring the angle defined by the plane transecting two daughter nuclei relative to the plane of the basement membrane, as indicated by integrin (CD104/ β4 or CD49f/ α6 staining) or nidogen staining. Differential gene expression analyses were performed in GenePattern[59] and expression data were visualized in Matlab. Radial histograms of division angle were plotted in Matlab from raw data binned into 10° increments. All other graphs were prepared in Prism 6. Figures were prepared using Adobe Photoshop and Illustrator CS6.

Supplementary Material

Refer to Web version on PubMed Central for supplementary material.

Acknowledgements

We thank Slobodan Beronja, Eva Hernando-Monge, Pedro Lee, Panagiotis Ntziachristos, Scott Williams, and Eva Gonzalez for discussions and comments on the manuscript. We thank Elaine Fuchs for generous support and reagents, and Paul Khavari for LZRS-Ras^{G12V}. We are grateful for the help received from the NYU's Flow Cytometry, the Biorepository, Histology and Microscopy Core facilities (NCRR S10 RR024708), and NYU's Division of Laboratory Animal Resources, an ALAAC-accredited mouse facility, for their expert handling and care of the mice. This research was also supported by grants to M.S. by the National Institutes of Health R00-AR057260 and NIH/NCRR 1UL1RR029893-01.

References

1. Clarke MF, et al. Cancer stem cells--perspectives on current status and future directions: AACR Workshop on cancer stem cells. Cancer Res. 2006; 66:9339–9344. [PubMed: 16990346]
2. Clarke MF, Fuller M. Stem Cells and Cancer: Two Faces of Eve. Cell. 2006; 124:1111–1115. [PubMed: 16564000]
3. Jaks V, Kasper M, Toftgard R. The hair follicle-a stem cell zoo. Exp. Cell Res. 2010; 316:1422–1428. [PubMed: 20338163]
4. Blanpain C, Fuchs E. Epidermal homeostasis: a balancing act of stem cells in the skin. Nat. Rev. Mol. Cell Biol. 2009; 10:207–217. [PubMed: 19209183]
5. Mascre G, et al. Distinct contribution of stem and progenitor cells to epidermal maintenance. Nature. 2012
6. Jensen KB, et al. Lrig1 expression defines a distinct multipotent stem cell population in mammalian epidermis. Cell Stem Cell. 2009; 4:427–439. [PubMed: 19427292]
7. Jaks V, et al. Lgr5 marks cycling, yet long-lived, hair follicle stem cells. Nat Genet. 2008; 40:1291–1299. [PubMed: 18849992]
8. Snippert HJ, et al. Lgr6 marks stem cells in the hair follicle that generate all cell lineages of the skin. Science. 2010; 327:1385–1389. [PubMed: 20223988]
9. Cotsarelis G, Sun TT, Lavker RM. Label-retaining cells reside in the bulge area of pilosebaceous unit: implications for follicular stem cells, hair cycle, and skin carcinogenesis. Cell. 1990; 61:1329–1337. [PubMed: 2364430]
10. Oshima H, Rochat A, Kedzia C, Kobayashi K, Barrandon Y. Morphogenesis and renewal of hair follicles from adult multipotent stem cells. Cell. 2001; 104:233–245. [PubMed: 11207364]
11. Tumbar T, et al. Defining the epithelial stem cell niche in skin. Science. 2004; 303:359–363. [PubMed: 14671312]
12. Morris RJ, et al. Capturing and profiling adult hair follicle stem cells. Nat Biotechnol. 2004; 22:411–417. [PubMed: 15024388]

13. Lien W-H, et al. Genome-wide Maps of Histone Modifications Unwind In Vivo Chromatin States of the Hair Follicle Lineage. Cell Stem Cell. 2011; 9:219–232. [PubMed: 21885018]
14. Blanpain C, Lowry WE, Geoghegan A, Polak L, Fuchs E. Self-renewal, multipotency, and the existence of two cell populations within an epithelial stem cell niche. Cell. 2004; 118:635–648. [PubMed: 15339667]
15. Greco V, et al. A two-step mechanism for stem cell activation during hair regeneration. Cell Stem Cell. 2009; 4:155–169. [PubMed: 19200804]
16. Bailleul B, et al. Skin hyperkeratosis and papilloma formation in transgenic mice expressing a ras oncogene from a suprabasal keratin promoter. Cell. 1990; 62:697–708. [PubMed: 1696852]
17. White AC, et al. Defining the origins of Ras/p53-mediated squamous cell carcinoma. Proc. Natl. Acad. Sci. U.S. A. 2011; 108:7425–7430. [PubMed: 21502519]
18. Lapouge G, et al. Identifying the cellular origin of squamous skin tumors. Proc. Natl. Acad. Sci. U.S.A. 2011; 108:7431–7436. [PubMed: 21502497]
19. Pierce GB, Wallace C. Differentiation of malignant to benign cells. Cancer Res. 1971; 31:127–134. [PubMed: 5545265]
20. Schober M, Fuchs E. Tumor-initiating stem cells of squamous cell carcinomas and their control by TGF-{beta} and integrin/focal adhesion kinase (FAK) signaling. Proc. Natl. Acad. Sci. U.S. A. 2011
21. Lapouge G, et al. Skin squamous cell carcinoma propagating cells increase with tumour progression and invasiveness. Embo J. 2012
22. Rhee H, Polak L, Fuchs E. Lhx2 maintains stem cell character in hair follicles. Science. 2006; 312:1946–1949. [PubMed: 16809539]
23. Chen T, et al. An RNA interference screen uncovers a new molecule in stem cell self-renewal and long-term regeneration. Nature. 2012
24. Horsley V, Aliprantis A, Polak L, Glimcher L, Fuchs E. NFATc1 Balances Quiescence and Proliferation of Skin Stem Cells. Cell. 2008; 132:299–310. [PubMed: 18243104]
25. Wu X, et al. Opposing roles for calcineurin and ATF3 in squamous skin cancer. Nature. 2010; 465:368–372. [PubMed: 20485437]
26. Young RA. Control of the embryonic stem cell state. Cell. 2011; 144:940–954. [PubMed: 21414485]
27. Rheinwald JG, Beckett MA. Tumorigenic keratinocyte lines requiring anchorage and fibroblast support cultures from human squamous cell carcinomas. Cancer Res. 1981; 41:1657–1663. [PubMed: 7214336]
28. Giard DJ, et al. In vitro cultivation of human tumors: establishment of cell lines derived from a series of solid tumors. J Natl Cancer I. 1973; 51:1417–1423.
29. Arnold K, et al. Sox2(+) adult stem and progenitor cells are important for tissue regeneration and survival of mice. Cell Stem Cell. 2011; 9:317–329. [PubMed: 21982232]
30. Lesko MH, Driskell RR, Kretzschmar K, Goldie SJ, Watt FM. Sox2 modulates the function of two distinct cell lineages in mouse skin. Dev. Biol. 2013
31. Bass AJ, et al. SOX2 is an amplified lineage-survival oncogene in lung and esophageal squamous cell carcinomas. Nat Genet. 2009; 41:1238–1242. [PubMed: 19801978]
32. Gen Y, et al. SOX2 identified as a target gene for the amplification at 3q26 that is frequently detected in esophageal squamous cell carcinoma. Cancer Genet. Cytogenet. 2010; 202:82–93. [PubMed: 20875870]
33. Bardot ES, et al. Polycomb subunits Ezh1 and Ezh2 regulate the Merkel cell differentiation program in skin stem cells. Embo J. 2013; 32:1990–2000. [PubMed: 23673358]
34. Beronja S, Livshits G, Williams S, Fuchs E. Rapid functional dissection of genetic networks via tissue-specific transduction and RNAi in mouse embryos. Nat Med. 2010; 16:821–827. [PubMed: 20526348]
35. Dajee M, et al. NF-kappaB blockade and oncogenic Ras trigger invasive human epidermal neoplasia. Nature. 2003; 421:639–643. [PubMed: 12571598]
36. Chen X, et al. Integration of external signaling pathways with the core transcriptional network in embryonic stem cells. Cell. 2008; 133:1106–1117. [PubMed: 18555785]

37. Ferrara N, Gerber H-P, LeCouter J. The biology of VEGF and its receptors. Nat Med. 2003; 9:669–676. [PubMed: 12778165]
38. Rittling SR, Chen Y, Feng F, Wu Y. Tumor-derived osteopontin is soluble, not matrix associated. J Biol Chem. 2002; 277:9175–9182. [PubMed: 11741994]
39. Png KJ, Halberg N, Yoshida M, Tavazoie SF. A microRNA regulon that mediates endothelial recruitment and metastasis by cancer cells. Nature. 2012; 481:190–194. [PubMed: 22170610]
40. Beck B, et al. A vascular niche and a VEGF-Nrp1 loop regulate the initiation and stemness of skin tumours. Nature. 2011; 478:399–403. [PubMed: 22012397]
41. Lichtenberger BM, et al. Autocrine VEGF signaling synergizes with EGFR in tumor cells to promote epithelial cancer development. Cell. 2010; 140:268–279. [PubMed: 20141840]
42. Driessens G, Beck B, Caauwe A, Simons BD, Blanpain C. Defining the mode of tumour growth by clonal analysis. Nature. 2012:1–5.
43. Malanchi I, et al. Cutaneous cancer stem cell maintenance is dependent on β-catenin signalling. Nature. 2008; 452:650–653. [PubMed: 18385740]
44. Kadoch C, Crabtree GR. Reversible disruption of mSWI/SNF (BAF) complexes by the SS18-SSX oncogenic fusion in synovial sarcoma. Cell. 2013; 153:71–85. [PubMed: 23540691]
45. Watanabe H, et al. SOX2 and p63 colocalize at genetic loci in squamous cell carcinomas. J. Clin. Invest. 2014; 124:1636–1645. [PubMed: 24590290]
46. Sarkar A, Hochedlinger K. The sox family of transcription factors: versatile regulators of stem and progenitor cell fate. Cell Stem Cell. 2013; 12:15–30. [PubMed: 23290134]
47. Sibilia M, et al. The EGF receptor provides an essential survival signal for SOS-dependent skin tumor development. Cell. 2000; 102:211–220. [PubMed: 10943841]
48. Lechler T, Fuchs E. Asymmetric cell divisions promote stratification and differentiation of mammalian skin. Nature. 2005; 437:275–280. [PubMed: 16094321]
49. Williams SE, Beronja S, Pasolli HA, Fuchs E. Asymmetric cell divisions promote Notch-dependent epidermal differentiation. Nature. 2011; 470:353–358. [PubMed: 21331036]
50. Tomasetti C, Levy D. Role of symmetric and asymmetric division of stem cells in developing drug resistance. Proc. Natl. Acad. Sci. U.S.A. 2010; 107:16766–16771. [PubMed: 20826440]
51. Hanahan D, Weinberg RA. The hallmarks of cancer. Cell. 2000; 100:57–70. [PubMed: 10647931]
52. Wiederschain D, et al. Single-vector inducible lentiviral RNAi system for oncology target validation. Cell Cycle. 2009; 8:498–504. [PubMed: 19177017]
53. Nowak JA, Fuchs E. Isolation and culture of epithelial stem cells. Methods Mol. Biol. 2009; 482:215–232. [PubMed: 19089359]
54. Rheinwald JG. Serial cultivation of normal human epidermal keratinocytes. Methods Cell Biol. 1980; 21A:229–254. [PubMed: 6157968]
55. Kent WJ, et al. The human genome browser at UCSC. Genome Res. 2002; 12:996–1006. [PubMed: 12045153]
56. Zhang Y, et al. Model-based analysis of ChIP-Seq (MACS). Genome Biol. 2008; 9:R137. [PubMed: 18798982]
57. Rendl M, Lewis L, Fuchs E. Molecular dissection of mesenchymal-epithelial interactions in the hair follicle. PLoS Biol. 2005; 3:e331. [PubMed: 16162033]
58. Tsai S-Y, et al. Oct4 and klf4 reprogram dermal papilla cells into induced pluripotent stem cells. Stem Cells. 2010; 28:221–228. [PubMed: 20014278]
59. Reich M, et al. GenePattern 2.0. Nat. Genet. 2006; 38:500–501. [PubMed: 16642009]

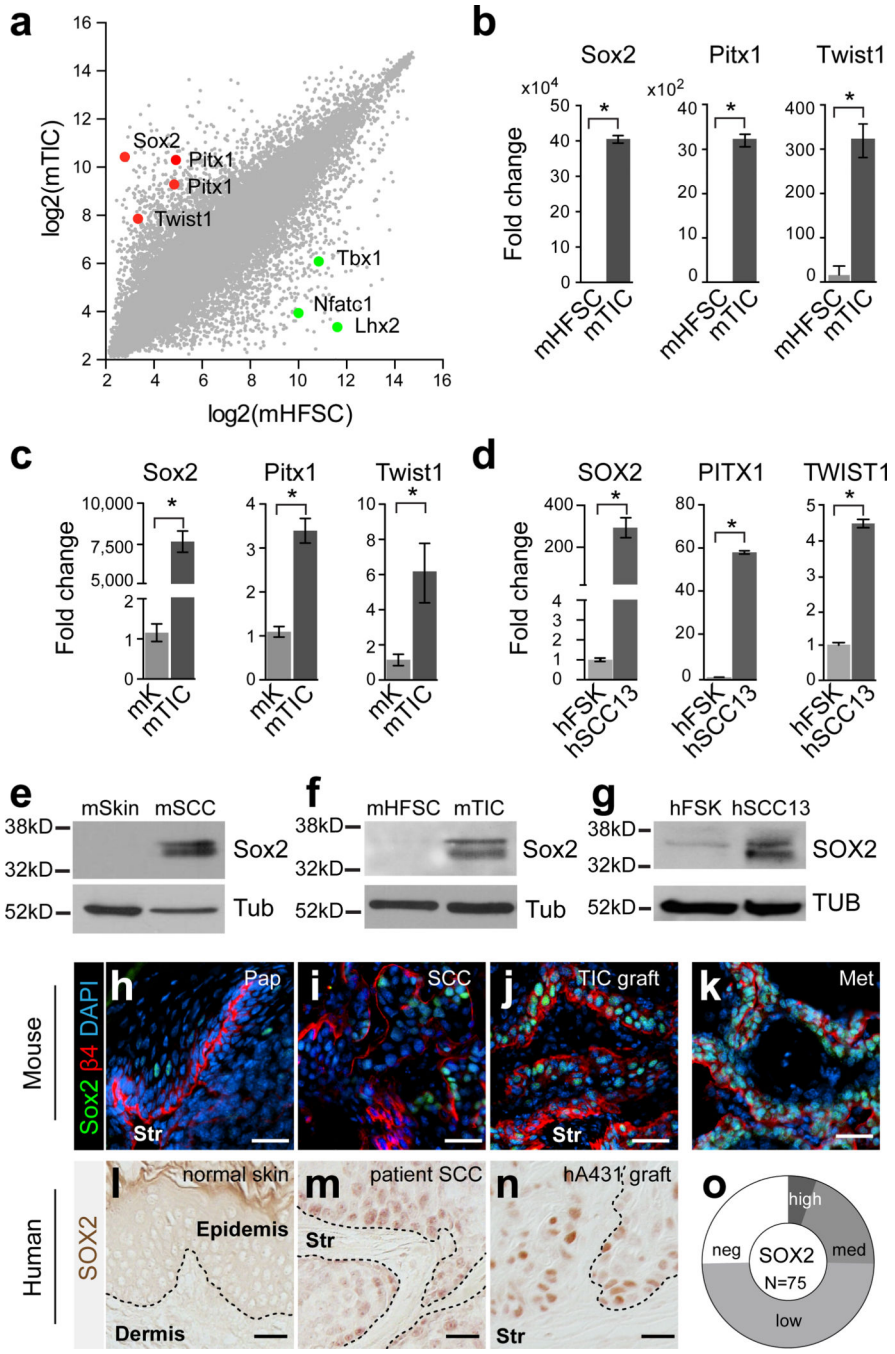

Figure 1. SOX2 expression distinguishes TICs from normal skin epithelial cells

(a) Scatter plot illustrating gene expression values of 45,101 transcripts in tumor-initiating cells (TIC) of murine (m) cutaneous squamous cell carcinoma (SCC) compared to hair follicle stem cells (HFSCs). Red and green dots indicate highly enriched transcription factors in mTICs and mHFSCs, respectively. **(b)** qRT-PCR analyses of Sox2, Pitx1, and Twist1 on RNA from freshly sorted mTICs and mHFSCs. **(c)** qRT-PCR analysis of Sox2, Pitx1, and Twist1 on RNA from cultured mTICs and mHFSCs. **(d)** qRT-PCR analysis of SOX2, PITX1, and TWIST1 on RNA from human foreskin (FSK) and SCC13 cultures. **(b–**

d) Data are represented as mean with error bars indicating ± s.d. (n=3, *P<0.05, Student's t-test). **(e–g)** Western blot analyses of Sox2 on total protein extracts from mSkin and mSCC **(e)**; cultured mHFSCs and mTIC **(f)**; and human foreskin keratinocyte (FSK) and SCC13 cultures **(g)**. β-Tubulin (Tub) was used as loading control. **(h–k)** Immunofluorescence microscopy of Sox2 (green) on benign mouse papillomas (**h**, Pap), primary mouse SCCs (**i**, SCC), orthotopic TIC transplants (**j**, TIC graft), and spontaneous lung metastases (**k**, Met). β4 integrin (red) demarcates the boundary between tumor epithelial cells and underlying stroma (Str). DAPI (blue) labels nuclear chromatin. **(l–n)** Immunohistochemistry of SOX2 on normal human skin **(l)**, primary human patient SCC **(m)**, and A431 xenograft **(n)**. **(o)** Donut chart summarizing SOX2 expression analysis on human cutaneous SCC tissue microarray. Nuclear SOX2 staining was detected in 75% of SCCs (56/75) with variable staining intensity (5% strong, 20% medium, 49% weak). **(h–n)** Scale bars are 50μm.

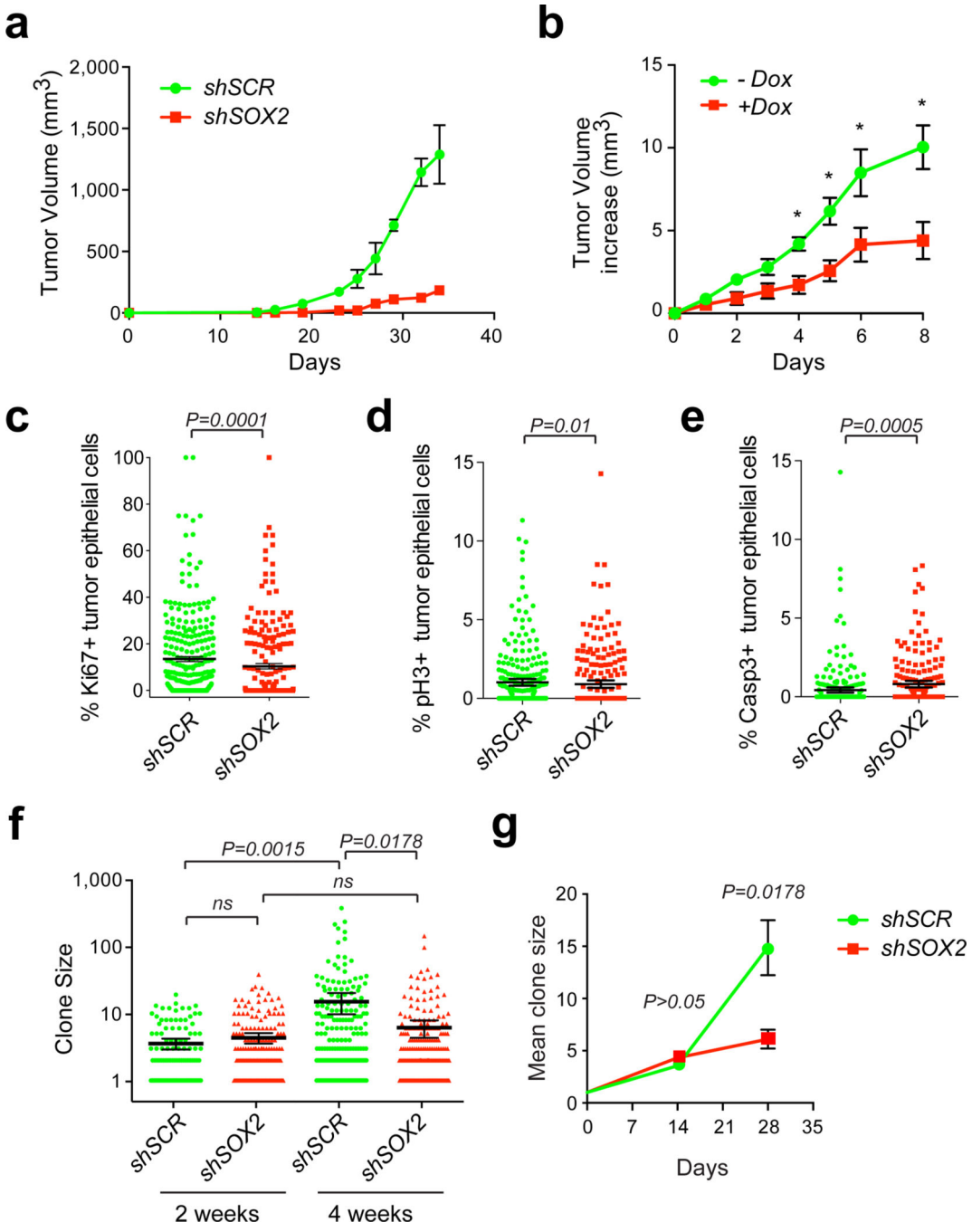

Figure 2. SOX2 is required for cutaneous SCC initiation and growth

(a) Tumor growth curves of human SCCs infected with lentivirus expressing short hairpin RNA (shRNA) against SOX2 along with nuclear red fluorescent protein (H2B-RFP; shSOX2) or scrambled control shRNA along with nuclear green fluorescent protein (H2B-GFP; shSCR) followed by transplantation onto Nude recipient mice. Data are represented as mean with error bars indicating ± s.e.m. (n=6, *P<0.05, Student's t-test). **(b)** Doxycycline-inducible knockdown of SOX2 in established human SCC xenografts. Data are represented as mean with error bars indicating ± s.e.m. (n=10, *P<0.05, Student's t-test). **(c–e)**

Quantitative analysis of proliferative Ki67 **(c)**, mitotic phospho-Histone H3(Ser10) pH3 **(d)**, and apoptotic activated Caspase-3 (Casp3) **(e)** positive cells in shSOX2;H2B-RFP or shSCR;H2B-GFP transduced A431 xenografts. Scatter plots illustrate the percentage of infected parenchymal cells that are positive for the respective marker in n>200 microscopic fields. Horizontal bars indicate mean ± 95% CI. (*P<0.05 Mann-Whitney non-parametric t-test). **(f–g)** Analysis of clonal growth competition assay at 2 and 4 weeks after intradermal transplantation when 1–2% of A431 cells have been transduced with shSOX2;H2B-RFP and shSCR;H2B-GFP (n=6). **(f)** Scatter plots illustrate clone size distributions. Horizontal lines represent mean with error bars indicating ± 95% CI. **(g)** Line graphs showing average clone size as a function of time (± s.e.m). **(f–g)** P values were obtained by Mann-Whitney non-parametric t-tests.

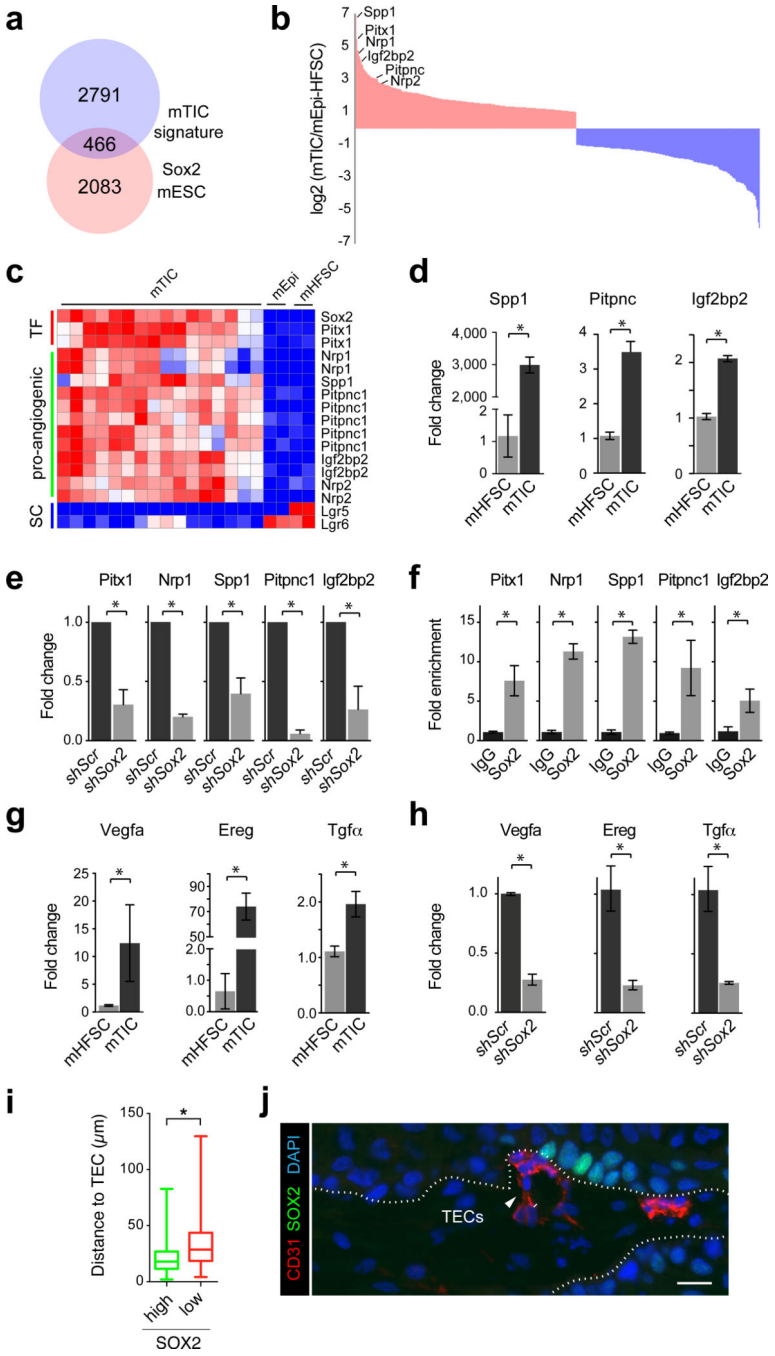

Figure 3. Sox2 promotes the expression of pro-angiogenic factors in tumor-initiating cells

(a) Venn diagram depicting overlap of 466 genes between the mouse TIC signature and a list of direct Sox2 targets in mouse ES cells. **(b)** Histogram illustrating the relative enrichment of 466 putative Sox2 target genes in mouse TICs compared to skin epithelial stem and progenitor cells. 254 genes are >2 fold upregulated (red) and 212 genes are >2-fold downregulated (blue). Pro-angiogenic molecules and Pitx1 are amongst the highest differentially expressed genes **(c)** Heat map exemplifying elevated expression of Pitx1 and pro-angiogenic factors, and the suppression of HFSC markers in TICs. **d**, qRT-PCR analysis

of Spp1, Pitpnc, and Igf2bp2 on TIC and HFSC cultures. **(e)** qRT-PCR analysis of Pitx1 and pro-angiogenic factors on mTIC cultures transduced with shScr or shSox2. **(f)** qRT-PCR analyses on chromatin samples from cultured mTICs after immunoprecipitation with anti-Sox2 and IgG control antibodies. **(g)** qRT-PCR analysis of EGF and VEGF signaling pathway components on primary mTICs and mHFSC cultures. **(h)** qRT-PCR analysis of EGF and VEGF signaling pathway components on mTIC cultures transduced with shScr or shSox2. **(d–h)** Bar graphs showing mean with error bars indicating ± s.d. (n=3, *P<0.05 Student's t-test) **(i)** Box and whisker plots describing measurements of the closest distance between TICs, expressing high or low levels of SOX2, and tumor endothelial cells (TECs). Bar indicates median, box indicates 25 and 75 percentile and whiskers indicate minimum and maximum measurements. **(j)** Representative image showing high-level SOX2-positive cells (green), TECs (CD31, red) and nuclear chromatin (DAPI, blue). White dotted line indicates tumor-stroma interface. Scale bar indicates 20 μm.

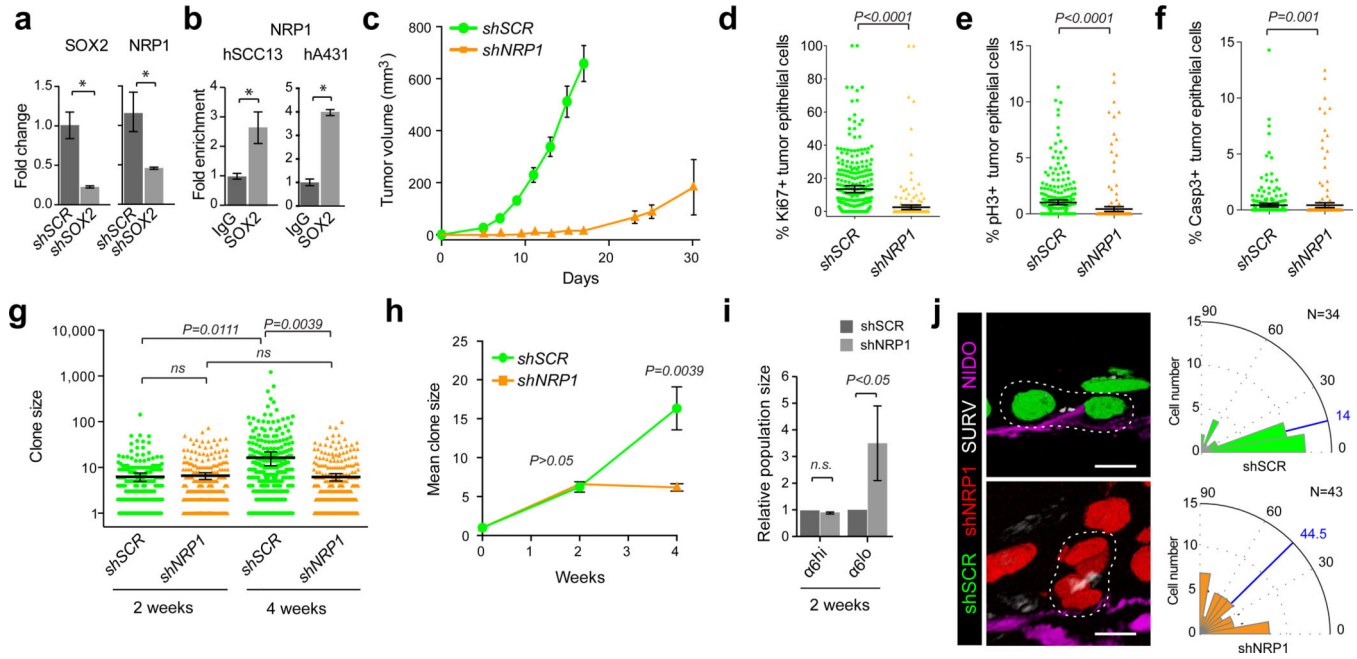

Figure 4. NRP1 expression is regulated by SOX2 and required for SCC growth

(a) qRT-PCR analysis of SOX2 and NRP1 on human SCC13 cells transduced with shSCR and shSOX2. **(b)** qRT-PCR analyses on chromatin samples from cultured human SCC13 and A431 cells after immunoprecipitation with anti-Sox2 and IgG control antibodies. **(a–b)** Bar graphs show mean with error bars indicating ± s.d (n=3, *P<0.05 Student's). **(c)** Tumor growth curves of A431 cells grafted onto Nude recipient mice after transduction with shNRP1;H2B-RFP or shSCR;H2B-GFP. Data are represented as mean with error bars indicating ± s.e.m. (n=6, *P<0.05, Student's t-test). **(d–f)** Quantitative analysis of proliferative Ki67 **(d)**, mitotic phospho-Histone H3(Ser10) pH3 **(e)**, and apoptotic activated Caspase-3 (Casp3) **(f)** positive cells in shNRP1;H2B-RFP or shSCR;H2B-GFP transduced A431 xenografts. Scatter plots illustrate the percentage of infected parenchymal cells that are positive for the respective marker in n>200 microscopic fields. Horizontal bars indicate mean ± 95% CI. (*P<0.05, Mann-Whitney non-parametric t-test). **(g,h)** Analysis of clonal growth competition assays at 2 and 4 weeks after intradermal transplantation when 1–2% of A431 cells have been transduced with shNRP1;H2B-RFP and shSCR;H2B-GFP (n=6). **(g)** Scatter plots illustrate clone size distributions. Horizontal lines represent mean with error bars indicating ± 95% CI. **(h)** Line graphs show average clone size as a function of time (± s.e.m). **(g–h)** P values were obtained by Mann-Whitney non-parametric t-tests. **(i)** Flow cytometric analyses of basement membrane-associated clones (integrin $\alpha6^{hi}$) in clonal competition assays two weeks after transplantation. Bar graphs show mean population size of shNRP1;H2B-RFP and shSCR;H2B-GFP expressing cells within the α6-integrin-high and α6-integrin-low gates. Error bars indicate ± s.d (n=6, *P<0.05, Student's t-test). **(j)** Projections of representative three-dimensional immunofluorescence micrographs (left) and radial histograms (right) indicating the orientation of basal cell divisions relative to the tumor-stroma interface in shSCR;H2B-GFP control (top, n=34) and shNRP1;H2B-RFP (bottom, n=43) human A431 SCC grafts. Survivin marks the spindle mid-body (SURV, white) and Nidogen (NIDO, magenta) demarcates the basement membrane. Scale bars

indicate 10 μm. Blue lines indicate median division angles. Statistical significance $P<0.01$ was determined by Mann-Whitney non-parametric t-test.

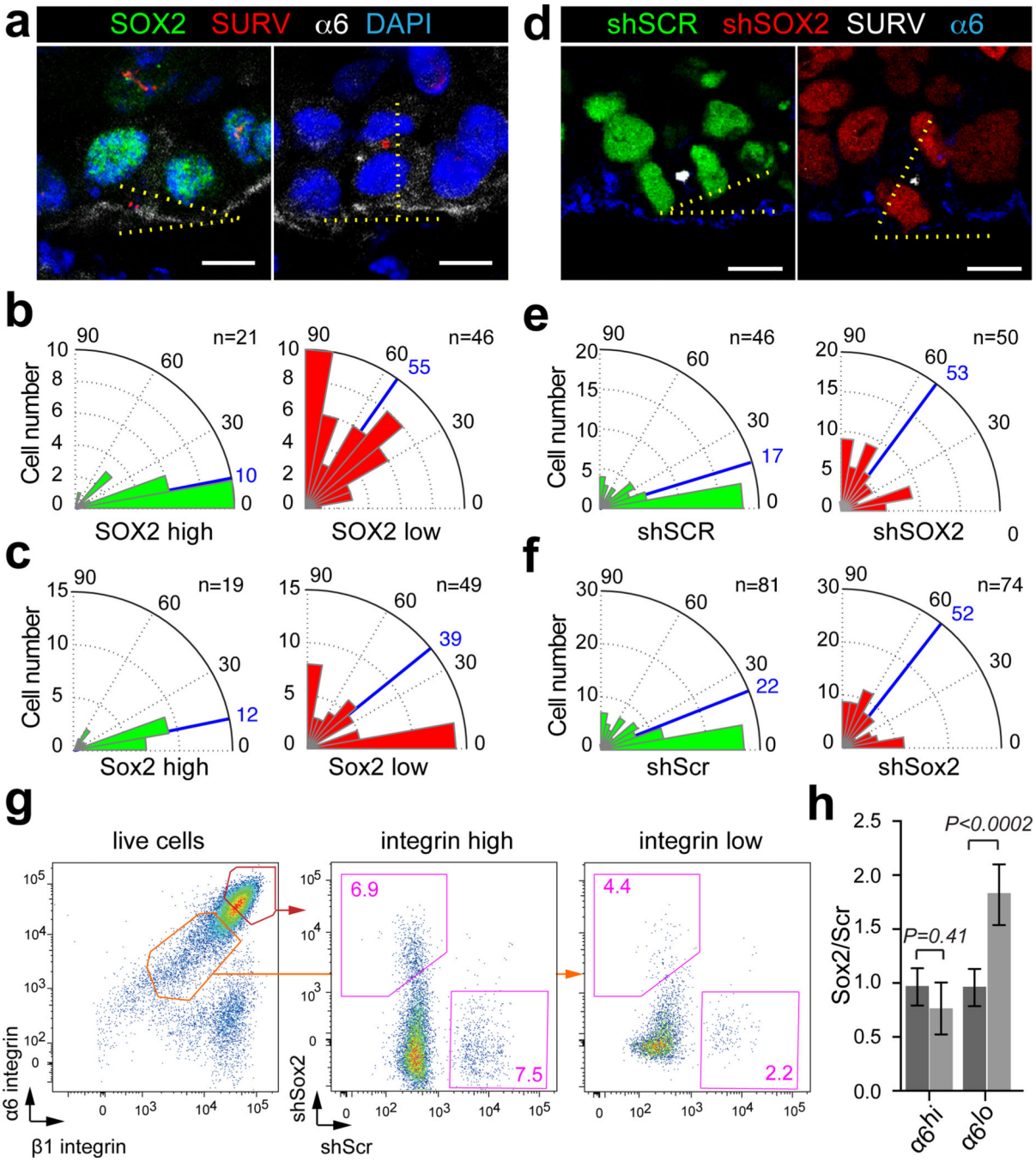

Figure 5. SOX2 expression promotes TIC divisions along the tumor-stroma interface

(a) Confocal sections of human SCCs stained with SOX2 (green), Survivin (SURV, red), α6-integrin (α6, white) and DAPI (blue). Scale bars indicate 10 μm. **(b–c)** Radial histograms indicating the orientation of basal cell divisions relative to the tumor-stroma interface expressing high (green) or low (red) levels of SOX2 in human **(b)** and mouse **(c)** SCCs. Blue lines indicate median division angles. **(d)** Projections of representative three-dimensional immunofluorescence micrographs of shSCR;H2B-GFP and shSOX2;H2B-RFP clones in A431 xenografts stained with Survivin (SURV, white), α6-integrin (blue). Scale bars

indicate 10 μm. **(e–f)** Radial histograms describe the orientation of basal cell divisions relative to the tumor-stroma interface in shSCR;H2B-GFP (green) and shSOX2;H2B-RFP (red) clones in human **(e)** and mouse **(f)** SCC transplants. Blue lines indicate median division angles. **(g–h)** Flow cytometric analyses of shSCR;H2B-GFP and shSOX2;H2B-RFP clonal competition assays two weeks after transplantation. **(g)** Scatter plots illustrate the relative abundance of shSCR;H2B-GFP and shSOX2;H2B-RFP cells within the α6/β1-integrin high and low gates. **(h)** Bar graphs show mean population size of shSOX2;H2B-RFP and shSCR;H2B-GFP expressing cells within the α6-integrin-high and α6-integrin-low gates with error bars indicating ± s.d (n=6, *P<0.05, Student's t-test).